

Genesis of Polyatomic Molecules in Dark Clouds: CO₂ Formation on Cold Amorphous Solid Water

Meenu Upadhyay and Marco Pezzella and Markus Meuwly*

*Department of Chemistry, University of Basel, Klingelbergstrasse 80 , CH-4056 Basel,
Switzerland.*

E-mail: m.meuwly@unibas.ch

June 16, 2021

Abstract

Understanding the formation of molecules under conditions relevant to interstellar chemistry is fundamental to characterize the chemical evolution of the universe. Using reactive molecular dynamics simulations with model-based or high-quality potential energy surfaces provides a means to specifically and quantitatively probe individual reaction channels at a molecular level. The formation of CO₂ from collision of CO(¹Σ) and O(¹D) is characterized on amorphous solid water (ASW) under conditions typical in cold molecular clouds. Recombination takes place on the sub-nanosecond time scale and internal energy redistribution leads to stabilization of the product with CO₂ remaining adsorbed on the ASW on extended time scales. Using a high-level, reproducing kernel-based potential energy surface for CO₂, formation into and stabilization of CO₂ and COO is observed.

The formation and chemical evolution of stars and galaxies is intimately linked to the presence of molecules.¹ This “Molecular Universe”^{1,2} requires molecules to be generated “bottom-up” but also involves them to be destroyed “top-down” by reaction channels that are potentially specific to the conditions in the interstellar medium. For the formation of neutrals, grain-surface chemistry involving interstellar ices inside dense molecular clouds is of particular importance.¹ Reactions on icy surfaces occur at the diffusion limit and their efficiency depends primarily on the diffusion of one or several of the reacting species on the surface and whether or not particular reaction channels involve entrance barriers. In dense cold clouds, CO is the main carbon reservoir¹ and the second most abundant molecule in Molecular Clouds with an important role as a molecular tracer for probing and characterizing the chemical and physical conditions of the environment.³

Observations indicate that the abundances of H₂O and CO₂ on grains within clouds are sufficient to be detected in the interstellar medium.^{4,5} The chemical precursor for formation of CO₂ is believed to be carbon monoxide. Thermoluminescence experiments of added CO to photolyzed N₂O in an Argon matrix at 7 K suggested that the O(³P)+CO(¹Σ⁺) reaction yields excited CO₂^{*} which, after emission of a photon, leads to formation of CO₂.⁶ Such a process has also been proposed to occur on interstellar grains⁷ and confirmed experimentally⁸ with an estimated entrance barrier of 0.014 eV to 0.103 eV for the process on ASW, compared with a value of 0.3 eV from high-level electronic structure calculations.⁹ The surrounding water matrix should facilitate relaxation of the ³A' or ³A'' states of CO₂ to the ¹A' ground state (correlating with linear ¹Σ_g⁺). On the other hand, the presence of an entrance barrier for the O(³P)+CO(¹Σ⁺) reaction has one led to consider the alternative CO+OH pathway for CO₂ formation¹⁰ which was, however, reconsidered to yield the HOCO intermediate in such environments in more recent experiments.¹¹

For atomic oxygen the possibility for diffusion on and within amorphous solid water (ASW)

was demonstrated down to temperatures of 10 K and 50 K from both, experiments and simulations.¹²⁻¹⁴ Typical temperatures of dense cold clouds have been estimated at ~ 15 K.¹⁵ The oxygen mobility found even at such low temperatures¹² opens up ways to form small molecules, including O₂, O₃, or CO₂ through atom/atom or atom/molecule recombination. In this context it is also of interest to note that excited O(¹D) state has been reported to be considerably more mobile than ground state O(³P).^{16,17} For molecular oxygen it was shown that both, ground and excited state O₂ can be stabilized on amorphous solid water.^{18,19}

Direct, barrierless recombination into the ground state of CO₂ is possible from O(¹D)+CO(¹Σ⁺). Excited O(¹D) can be formed from photolysis of H₂O²⁰ and the radiative lifetime is 110 minutes.²¹ Also, neutral dissociation of water into H₂ and O(¹D) in the presence of CO has recently been reported to lead to formation of CO₂ in cryogenic films containing CO and H₂O.²² Here, the reaction O(¹D)+CO(¹Σ⁺) → CO₂(¹Σ_g⁺) on the surface of ASW is investigated at a molecular level. Two potential energy surfaces (PESs) are used to describe the energetics of CO+O → CO₂ formation (see Supporting Information for the energy functions used). One is a Morse-Morse-Harmonic (MMH) parametrization based on multi-reference CI calculations for CO-dissociation, fitted to a Morse functional form together with an empirical parametrization for the OCO angle θ . The second PES is a 3-dimensional reproducing kernel Hilbert space (RKHS) representation of CCSD(T)-F12 calculations which (see Figure S1 for the quality of the representation) is more accurate than the MMH PES but also considerably more computationally expensive to evaluate. Energy conservation for MD simulations using both PESs is reported in Figure S2.

The 3-dimensional MMH-PES, fit to MRCI/aug-cc-pVTZ data, is qualitatively correct.⁹ The equilibrium geometry is a linear O-C-O configuration with C-O distances of 1.1644 Å with bending, symmetric and asymmetric stretching frequencies at 645 cm⁻¹, 1226 cm⁻¹ and 2450 cm⁻¹, respectively, compared with 667 cm⁻¹ for bend, 1333 cm⁻¹ for symmetric stretch and

2349 cm^{-1} for asymmetric stretch.²³

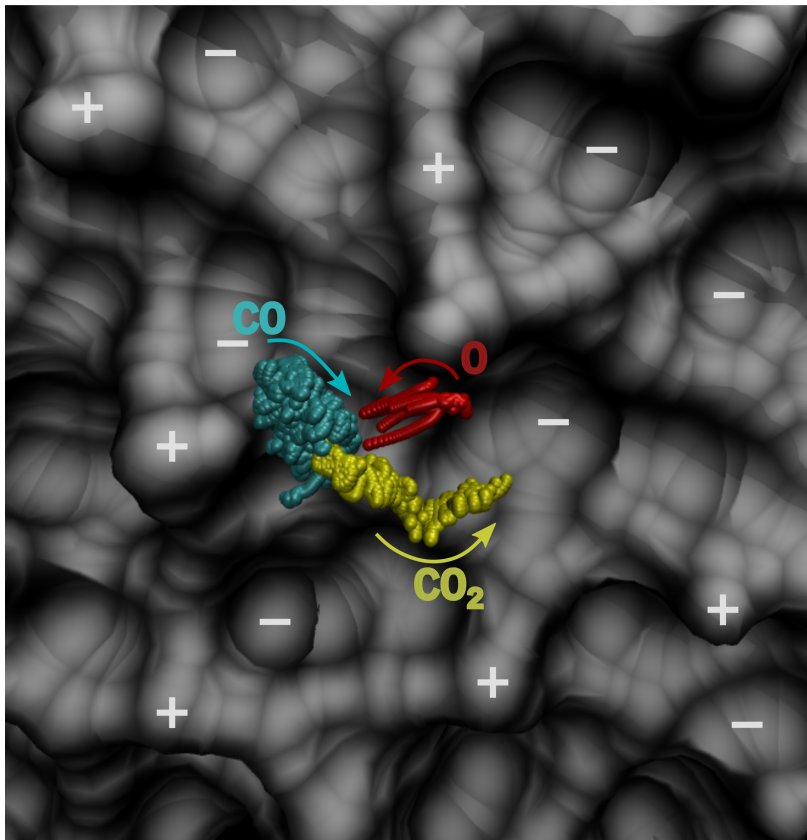


Figure 1: Trajectories leading to CO_2 recombination. The O-atom (red) and CO molecule (cyan) from 8 different trajectories are shown to form CO_2 (yellow). Before and after recombination all species diffuse on the ASW (grey colors) surface. The “plus” and “minus” signs indicate protuberances and indentations of the ASW surface.

First, recombination simulations were run with the MMH model. This provides a qualitatively correct description of the CO_2 formation dynamics at reduced computational cost. Typical recombination trajectories projected onto the ASW surface are shown in Figure 1. Before recombination, CO (cyan) and O (red) diffuse separately in their respective adsorption sites on the ASW. After recombination, CO_2 (yellow) continues to diffuse on the ASW.

A representative time series for $\text{CO}_A + \text{O}_B$ to form CO_2 is reported in Figure 2. From an initial separation of $R = 4.66 \text{ \AA}$ and $\theta = 135^\circ$, CO_2 is formed within $\sim 8 \text{ ps}$ (inset of Figure

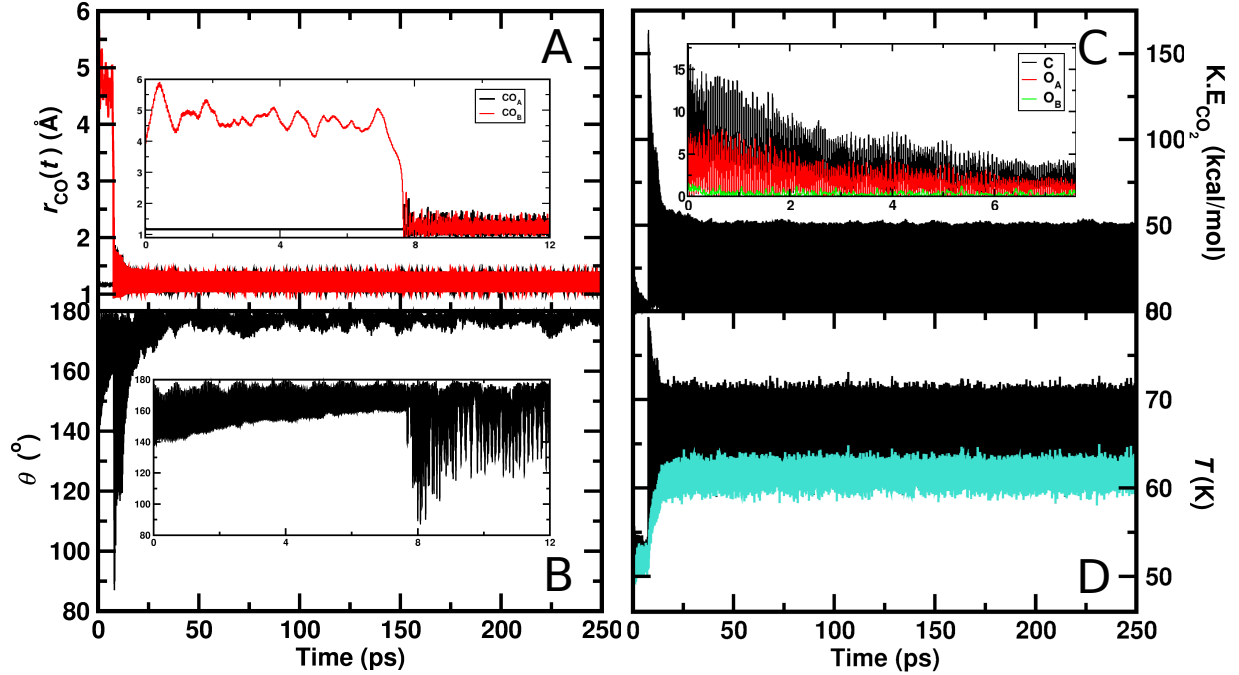


Figure 2: Interatomic distances CO_A and CO_B (panel A) and the OCO angle θ (panel B, running average) from a 250 ps simulation using the MMH PES. Initially, $R = 4.66 \text{ \AA}$ and $\theta = 135^\circ$. The diffusive motion of O_B can be seen in the inset before recombination takes place after ~ 7 ps. After recombination both CO stretches are equally highly excited. Panel C: Kinetic energy of CO_2 along with the contribution from each of the atoms. Panel D: Average temperature of the ASW (cyan) and the full system (black) before and after CO_2 formation. After recombination there is a step increase in temperature of the entire system (CO_2 plus ASW) whereas warming of the ASW is more gradual. This suggests that the underlying process is vibrational relaxation of hot CO_2 on a cool ASW surface which gradually warms and assumes a new thermal equilibrium.

2A). Upon recombination, both CO stretch coordinates are highly excited and the OCO angle fluctuates around $\theta = 180^\circ$ with an amplitude of $\sim 10^\circ$ (Figures 2A and B). For the remaining 250 ps CO₂ relaxes slowly and remains as a diffusing product on the ASW (see also Figure 1).

It is also of interest to follow the kinetic energy and the temperature of the ASW before and after recombination, see Figures 2C and D. Before CO_A + O_B recombination the average temperature of the water molecules and the entire system are close to one another and fluctuate around 50 K. Upon recombination the temperatures as determined from the kinetic energies of the oxygen and carbon atoms increases considerably by about 10 K on average and assume different values as the system now consists of a “hot” CO₂ molecule adsorbed on a cool ASW surface. The temperature of the full system (recombined CO₂ and the ASW) first shows a prominent peak reaching 75 K right after recombination and relaxing subsequently. Contrary to that, the temperature of the water molecules does not show such a spike but rather increases gradually from 50 K to 60 K following relaxation of the CO₂ molecule (inset Figure 2D).

To better characterize relaxation of the internal energy, longer (20 ns) simulations were also run. Figure 3 reports the CO bond lengths (panel A), the OCO angle (panel B), the kinetic energy of CO₂ (panel C), and the temperatures of the total system (panel D, black) and the ASW (panel D, cyan). During the entire 20 ns slow relaxation of the CO stretch amplitudes takes place, interrupted by occasional large amplitude motions, caused by scattering of the CO₂ from collisions with the water molecules. Such collisions are accompanied by increase of the kinetic energy of the entire CO₂ molecule. The raw data for $\theta(t)$ is reported in Figure S3. Energy exchange between the vibrationally excited CO₂ molecule and the ASW surface continues out to 20 ns and beyond which is reflected in the continued warming of the water molecules. However, the slope of the cyan curve in Figure 3D is steeper during the first 5 ns

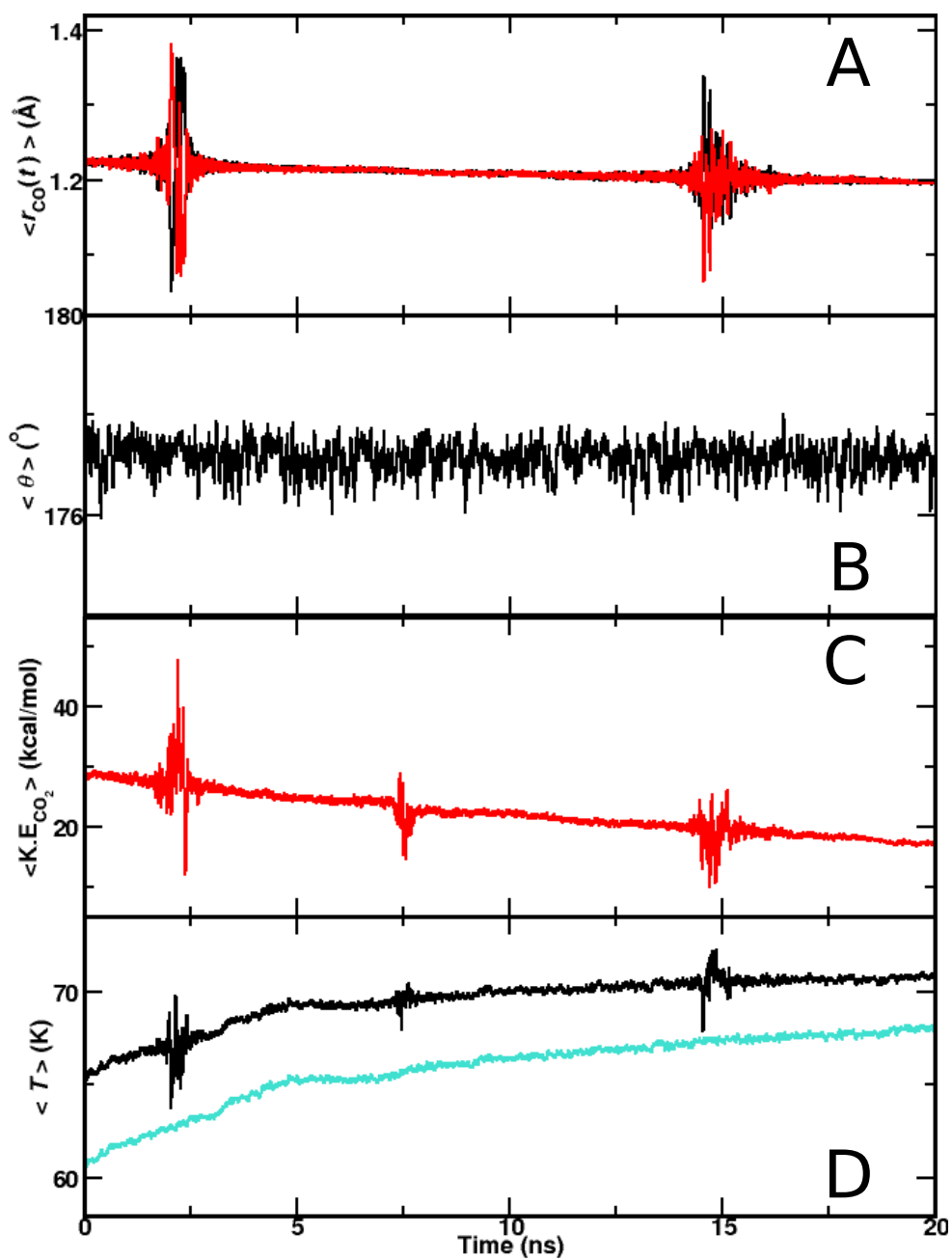


Figure 3: Interatomic distances CO_A and CO_B (panel A), OCO angle (panel B), kinetic energy of CO_2 (panel C) and ASW (cyan) and overall system (black)(panel D) from 20 ns simulation. The spikes are due to collisions of CO_2 with the surrounding water matrix.

and then flattens out for the remainder of this trajectory.

The MMH simulations discussed so far demonstrate that CO+O collisions lead to formation of CO₂ which relaxes on time scales longer than nanoseconds and does not desorb from the ASW surface.

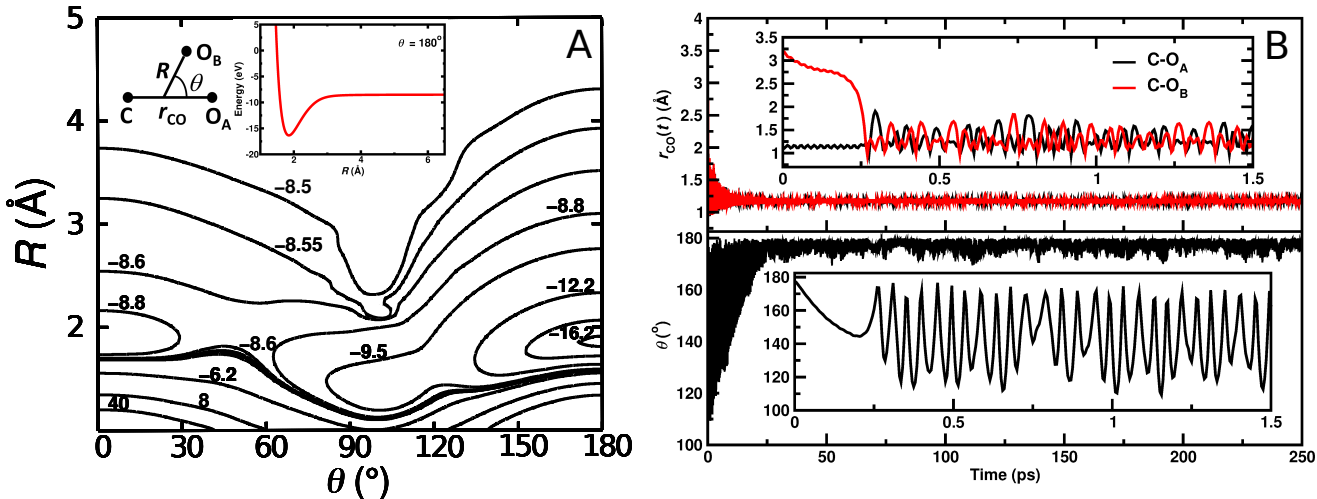


Figure 4: Panel A: Two-dimensional cut through the 3d RKHS PES at the CCSD(T)-F12 level of theory for the CO + O channel at fixed $r_{\text{CO}_A} = 1.21 \text{ \AA}$. The inset reports the 1d cut along $\theta = 180^\circ$ for $r_{\text{CO}_A} = 1.21 \text{ \AA}$. All energies in eV and the zero of energy at the dissociation into atomic fragments. Panel B: Interatomic distances CO_A and CO_B (top panel, for labels see panel A) and the OCO angle (bottom panel) from a 250 ps simulation with $R = 3.9 \text{ \AA}$ and $\theta = 180^\circ$ using the RKHS PES. Initially, the CO_A bond (black) is fluctuating around its thermal (50 K) equilibrium separation but the amplitude increases considerably after recombination due to internal vibrational relaxation. The OCO angle relaxes to a quasi-linear structure on the 25 ps time scale.

Corresponding simulations were carried out with the more realistic but computationally more expensive RKHS²⁴ representation of the CCSD(T)-F12 PES (see SI). Figure 4 reports the two dimensional PES for $r_{\text{CO}_A} = 1.21 \text{ \AA}$ and varying R and θ , and shows a deep minimum for the linear OCO structure ($\theta = 180^\circ$) together with the high-energy, metastable COO structure ($\theta = 0^\circ$), 167.7 kcal/mol higher in energy than the global minimum. Such a COO intermediate has been proposed from the interpretation of the C+O₂ reaction²⁵ and was also found in multiconfiguration SCF²⁶ and MRCI+Q calculations.⁹ The two structures are

separated by a barrier of 9.55 kcal/mol in going from the COO to the OCO structure.

A typical reactive trajectory to form CO₂ using the RKHS PES is reported in Figure 4B. Again, recombination leads to a highly vibrationally excited CO₂ molecule with rapidly decaying CO stretch amplitude for the CO-bond that is newly formed (red trace) whereas the CO_A vibrates around 1 Å initially and extends to ~ 1.2 Å upon recombination. The OCO angle relaxes to a quasi-linear structure on the 25 ps time scale, see lower panel in Figure 4B. As this 3-dimensional PES also supports a COO conformation, it is of interest to start simulations from initial orientations $\theta = 0^\circ$. Indeed, COO formation and stabilization on the sub-nanosecond time scale is observed, see Figure S4. Such an intermediate is of potential interest as it can lead to C + O₂ formation.

The possible final states after collision include (I) CO_A + O_B \rightarrow CO_A + O_B (flyby) (II) CO_A + O_B \rightarrow CO_B + O_A (atom exchange) (III) CO_A + O_B \rightarrow CO₂ (CO₂ formation) (IV) CO_A remains on the surface and O_B desorbs (elastic scattering (ES1)), (V) CO_A desorbs and O_B remains on the surface (ES2), and (VI) both, CO and O desorb from the ASW surface. For each of the initial conditions between 100 and 1000 independent trajectories were run, see Tables S1, S2 and S3. In total, 32500 simulations were run to determine the probability and rate for CO₂ formation depending on the initial conditions. All processes I to VI were observed in the simulations described in the following. One of the possible processes that was not observed on the nanosecond time scale is CO₂ formation with subsequent desorption of CO₂. This is reminiscent of the situation for O₂ formation for which desorption of molecular oxygen after oxygen atom recombination did not occur.¹⁸

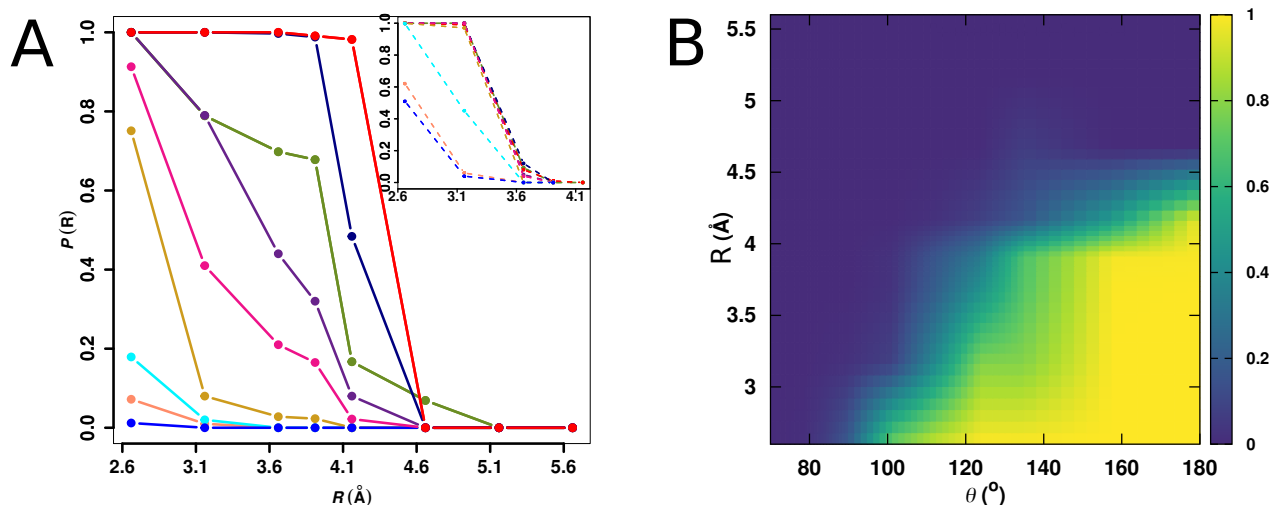


Figure 5: Panel A: The CO₂ formation probability as a function of R and θ normalized to the number of trajectories with Morse potential (main panel) and RKHS (inset) where different colors refer to probability for different angles. Color code: darkblue: 78.75°; salmon: 84.375°; skyblue: 90.0°, gold: 101.25°, pink: 112.5°, darkorchid: 123.75°, olive: 135.0°, navy: 157.5°, red: 180.0°. Panel B: Plot for the CO₂ formation probability as a function of R and θ using MMH PES. For a smoother shape of $P(R, \theta)$ kernel density estimation (KDE)²⁷ was used.

As the main focus of the present work concerns a) whether or not CO₂ is formed, b) whether CO₂ stabilizes and c) what other processes follow the recombination reaction, the initial separations between the two reaction partners to explore these questions was limited to $R \sim 6$ Å. As already found for the O(³P)–O(³P) reaction even initial separations of ~ 10 Å can lead to recombination, see Figure S4. However, to maintain simulation times manageable for this two-dimensional problem, the initial separations were limited to a somewhat shorter value of R .

Figure 5A reports the reaction probability for CO₂ formation depending on the initial reaction geometry (R, θ) for the MMH (main panel) and the RKHS PES (inset). Simulations starting from $\theta = 180^\circ$, i.e. along the O_AC–O_B approach have unit reaction probability with initial separations ranging from $R = 2.6$ Å up to $R = 4.5$ Å. Such separations cover both situations, the reacting partners within the same and in two different wells. Moving along θ it is found that on the MMH PES the reaction probabilities rapidly decrease whereas on the

RKHS PES they remain close to 1 up to $\theta \approx 100^\circ$ after which they decrease (inset Figure 5A). These differences are due to the different topographies of the two PESs.

For the MMH model there is a sufficient number of trajectories on a fine and extensive grid of initial collision geometries to also construct a 2-dimensional probability function for the reaction probability, see Figure 5B. This was done by using kernel density estimation²⁷ applied to the raw data from Figure 5A. It is found that as soon as the oxygen atom diffuses within a range of $\sim 4 \text{ \AA}$ of the center of mass of CO molecule, formation of CO₂ is highly probable.

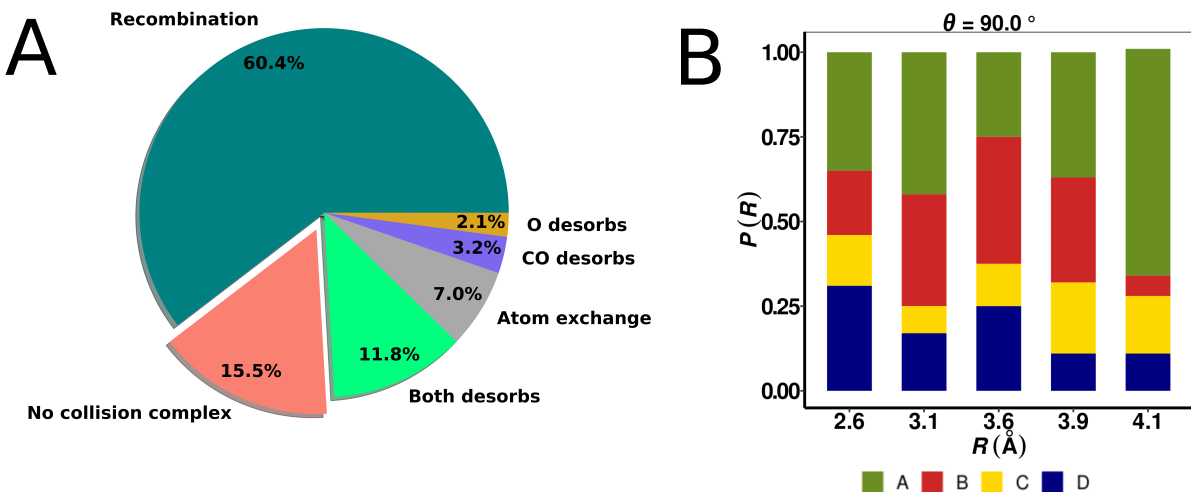


Figure 6: Panel A: Classification of outcomes from all the > 30000 simulations using the MMH PES. In more than half the cases CO₂ is formed whereas for 15 % of the cases the two collision partners do not meet. The remaining 25 % include atom exchange reactions, elastic scattering or desorption of both collision partners. Panel B: After atom exchange, there are 4 further possibilities i.e (A) both CO and O remain on the water surface, (B) both CO and O desorb, (C) O remains and CO desorbs, and (D) CO remains and O desorbs from the water surface for $\theta = 90^\circ$. See Figure S5 for different angles.

With respect to the distribution of the final state channels, more than 50 % of the trajectories run on the MMH PES lead to CO₂ and remain in this state, see Figure 6A. The multiple long-time (20 ns) simulations indicate that once formed, CO₂ is expected to remain adsorbed

on the ASW and vibrationally cools on considerably longer time scales (μs to ms). Among the other, minor, channels, the one not forming a collision complex is most probable (16 %), followed by desorption of both reaction partners (12 %), and the atom exchange reaction (7 %), whereas desorption of either CO or O occur rarely.

The atom exchange reaction is of particular interest because it provides another recombination channel, but probably on longer simulation times, if both reaction partners remain on the ASW. Figure 6B shows that CO_B and O_A remaining on the ASW after atom exchange (green) is most probable irrespective of the initial separation between CO_A and O_B . This is followed by desorption of both, whereas desorption of either CO_B or O_A is less likely on average. Thus, even if the initial collision process leads to atom exchange, there is still probability for subsequent CO_2 formation because both reaction partners remain on the ASW.

The present work demonstrates that CO_2 formation and stabilization from collision of CO and $\text{O}(\text{}^1\text{D})$ on ASW is possible and occurs on the sub-nanosecond time scale for the reaction partners within 10 Å. This compares with a radiative lifetime of 110 minutes²¹ of $\text{O}(\text{}^1\text{D})$ which can be formed from photolysis of H_2O .²⁰ Relaxation of the highly excited CO_2 product occurs on much longer time scales which is not covered here. From previous work on $\text{O}(\text{}^3\text{P})+\text{O}(\text{}^3\text{P})$ to form O_2 it is known that full vibrational relaxation occurs on the μs time scale.^{18,28} Similarly, it is expected that CO_2 vibrational relaxation extends out to considerably longer time scales than those covered in the present work (tens of ns). Using a flexible water model may provide additional channels to speed up vibrational relaxation of CO_2 , as was recently reported for O_2 on ASW.¹⁸ A fluctuating charge model to capture charge flow between the initial $\text{O}(\text{}^1\text{D})+\text{CO}(\text{}^1\Sigma^+)$ and the CO_2 final state is expected to lead to more rapid diffusion of the CO molecule and hence increased recombination rates (see SI).

Effects due to quantum nuclear dynamics are not included here but are expected to be small

given the large mass of the particles involved. In fact, earlier work¹⁴ has demonstrated that the experimentally¹² determined T -dependent mobility of $O(^3P)$ is a consequence of ASW surface roughness rather than tunneling at low temperature. Also, the validity of QCT-based simulations has been explicitly validated for the [CNO] reactive system by comparing final vibrational state distributions with time-independent quantum simulations.²⁹ The efficiency of non-adiabatic effects due to $O(^1D)$ to $O(^3P)$ conversion have been estimated⁹ to be 10 % at 300 K based on earlier measurements.³⁰ This may change at lower temperature, though, and explicit inclusion of nonadiabatic processes for the $O(^1D)+CO$ association reaction to form CO_2 appears to be of interest in the future.

The simulations on the RKHS PES support the possibility to form the COO isomer. Early emission spectra found that the $C(^3P) + O_2(^3\Sigma_g^-)$ reaction generates CO with $v' = 17$ and that the transition state has the COO configuration rather than OCO.³¹ As both, the high-level CCSD(T)-F12 PES and a recently determined MRCISD+Q/aug-cc-pVTZ ground state PES⁹ support stabilization of the COO structure, the present results also indicate that association of CO with $O(^1D)$ can lead to formation and stabilization of COO.

Complementary to the $O(^1D)+CO(^1\Sigma^+)$ reaction considered here, it is expected that the $O(^3P)+CO(^1\Sigma^+)$ process to yield triplet (excited) CO_2 is also feasible. The $O(^3P)+CO(^1\Sigma^+)$ asymptotic state connects to the excited $^3A'$ and $^3A''$ states of CO_2 both exhibiting entrance barriers of 0.2 eV and 0.3 eV in the gas phase, respectively, at the CASSCF-MP2 level of theory³² which change to 0.3 eV and 0.4 eV from MRCI+Q calculations.⁹ Experiments on ASW indicate that the entrance barrier reduces to between 0.014 and 0.067 eV.⁸ Furthermore, symmetry breaking due to the water environment⁶ makes the transition from triplet to singlet (ground state) CO_2 possible. For the $O(^3P)+CO(^1\Sigma^+)$ reaction equally accurate PESs are available⁹ which allow to follow this pathway at molecular detail.

Here, the reaction probability depends on both, the separation and orientation of the reacting partners. This differs from $O(^3P)+O(^3P)$ recombination to form O_2 and increases the conformational space to be sampled. Thus, initial separations were limited to $\sim 6 \text{ \AA}$ which, however, does not affect the generality of the present results. In fact, reactive trajectories were shown to still sample considerably larger separations ($R \sim 10 \text{ \AA}$) due to surface diffusion of the reactants before CO_2 formation occurred. It will be of interest to compare the current results with those from laboratory experiments along similar lines as was possible for oxygen atom recombination.¹² As an example, experiments involving $O(^1D)$ have been recently carried out with acetylene³³ and formation of CO_2 involving $O(^1D)$ on mixed CO/H_2O films has been reported to be the dominant reaction channel.

This work demonstrates that genesis of small polyatomic molecules can be investigated from computations using high-level electronic structure and molecular dynamics methods. For the specific case of CO_2 formation along the $O(^1D)+CO(^1\Sigma^+)$ asymptote the product stabilizes through intermolecular vibrational relaxation (IVR) and does not desorb from the ASW on the $< 100 \text{ ns}$ time scale. The fact that $O(^1D)$ with a radiative lifetime²¹ of 110 min is considerably more mobile than ground state $O(^3P)$ ^{16,17} should make this process to form CO_2 feasible. Furthermore, formation of the COO isomer is consistent with early gas-phase experiments. With recent advances in machine learning of reactive force fields for polyatomic molecules,³⁴⁻³⁶ explicit characterization of a wide range of molecule formation processes at low temperatures and under realistic conditions in interstellar space become possible. Such studies will ideally complement laboratory-based and observational astrochemistry efforts to better understand molecule abundances and the chemical evolution of molecular clouds.

Supporting Information

The supporting information reports Methods, Tables with a summary of all reactive simulations, and supporting figures for the present work.

Data Availability Statement

The data needed for the RKHS representation of the CCSD(T)-F12 PES is available at <https://github.com/MeuwlyGroup/co2.asw>.

Acknowledgments

This work was supported by the Swiss National Science Foundation grants 200021-117810, 200020-188724, the NCCR MUST, and the University of Basel which is gratefully acknowledged.

References

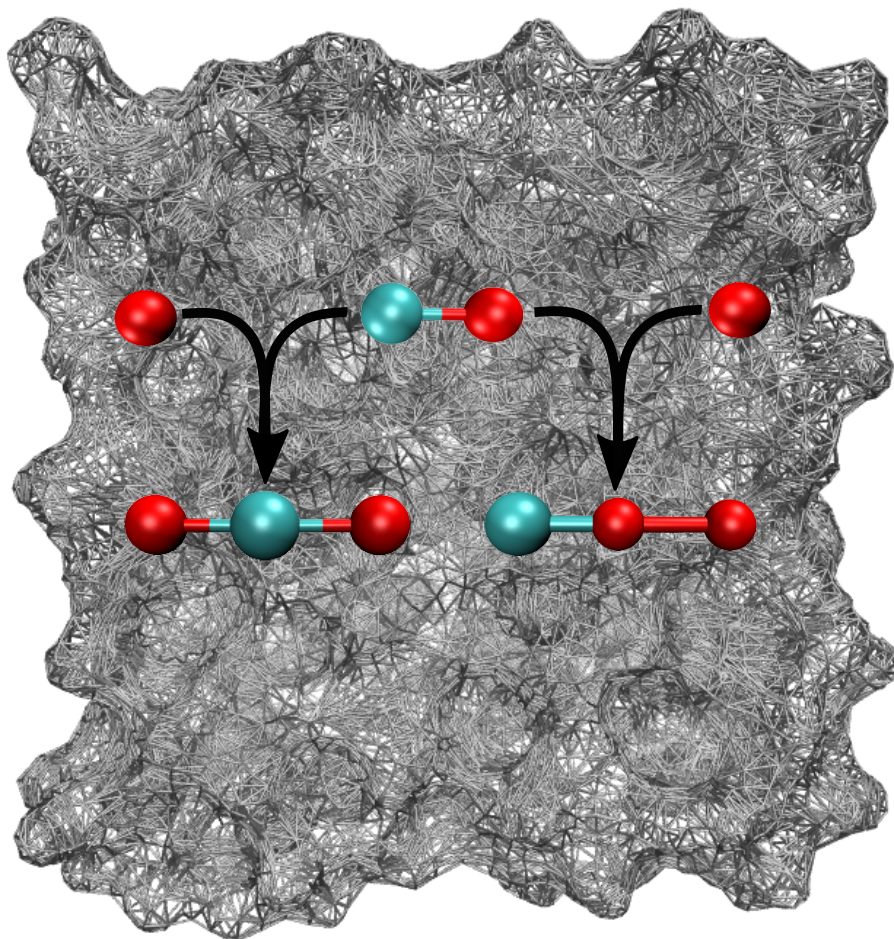
- (1) Tielens, A. G. G. M. The molecular universe. *Rev. Mod. Phys.* **2013**, *85*, 1021.
- (2) Tielens, A. G. G. M.; Hagen, W. Model Calculations of the Molecular Composition of Interstellar Grain Mantles. *Astron. Astrophys.* **1982**, *114*, 245–260.
- (3) Neininger, N.; Guélin, M.; Ungerechts, H.; Lucas, R.; Wielebinski, R. Carbon monoxide emission as a precise tracer of molecular gas in the Andromeda galaxy. *Nature* **1998**, *395*, 871–873.
- (4) Whittet, D.; Gerakines, P.; Hough, J.; Shenoy, S. Interstellar extinction and polarization

- in the Taurus dark clouds: the optical properties of dust near the diffuse/dense cloud interface. *Astrophys. J.* **2001**, *547*, 872.
- (5) Garrod, R. T.; Pauly, T. On the Formation of CO₂ and Other Interstellar Ices. *Astrophys. J.* **2011**, *735*, 15.
- (6) Fournier, J.; Deson, J.; Vermeil, C.; Pimentel, G. Fluorescence and thermoluminescence of N₂O, CO, and CO₂ in an argon matrix at low temperature. *J. Chem. Phys.* **1979**, *70*, 5726–5730.
- (7) Ruffle, D. P.; Herbst, E. New models of interstellar gas-grain chemistry - III. Solid CO₂. *Mon. Not. R. Astron. Soc.* **2001**, *324*, 1054–1062.
- (8) Minissale, M.; Congiu, E.; Manicò, G.; Pirronello, V.; Dulieu, F. CO₂ formation on interstellar dust grains: a detailed study of the barrier of the CO+ O channel. *Astron. Astrophys.* **2013**, *559*, A49.
- (9) San Vicente Veliz, J. C.; Koner, D.; Schwilk, M.; Bemish, R. J.; Meuwly, M. The C(³P) + O₂(³Σ_g⁻) ↔ CO₂ ↔ CO(¹Σ⁺) + O(¹D)/O(³P) Reaction: Thermal and Vibrational Relaxation Rates from 15 K to 20000 K. *Phys. Chem. Chem. Phys.* **2021**, *in print*, in print.
- (10) Ioppolo, S.; Van Boheemen, Y.; Cuppen, H.; Van Dishoeck, E.; Linnartz, H. Surface formation of CO₂ ice at low temperatures. *Mon. Not. R. Astron. Soc.* **2011**, *413*, 2281–2287.
- (11) Qasim, D.; Lamberts, T.; He, J.; Chuang, K.-J.; Fedoseev, G.; Ioppolo, S.; Boogert, A.; Linnartz, H. Extension of the HCOOH and CO₂ solid-state reaction network during the CO freeze-out stage: inclusion of H₂CO. *Astron. Astrophys.* **2019**, *626*, A118.
- (12) Minissale, M.; Congiu, E.; Baouche, S.; Chaabouni, H.; Moudens, A.; Dulieu, F.; Ac-

- colla, M.; Cazaux, S.; Manico, G.; Pirronello, V. Quantum Tunneling of Oxygen Atoms on Very Cold Surfaces. *Phys. Rev. Lett.* **2013**, *111*, 053201.
- (13) Lee, M. W.; Meuwly, M. Diffusion of atomic oxygen relevant to water formation in amorphous interstellar ices. *Faraday Discuss.* **2014**, *168*, 205–222.
- (14) Pezzella, M.; Unke, O. T.; Meuwly, M. Molecular Oxygen Formation in Interstellar Ices Does Not Require Tunneling. *J. Phys. Chem. Lett.* **2018**, *9*, 1822–1826.
- (15) Bergin, E. A.; Tafalla, M. Cold dark clouds: the initial conditions for star formation. *Annu. Rev. Astron. Astrophys.* **2007**, *45*, 339–396.
- (16) Danilychev, A.; Apkarian, V. Temperature induced mobility and recombination of atomic oxygen in crystalline Kr and Xe. I. Experiment. *J. Chem. Phys.* **1993**, *99*, 8617–8627.
- (17) Apkarian, V.; Schwentner, N. Molecular photodynamics in rare gas solids. *Chem. Rev.* **1999**, *99*, 1481–1514.
- (18) Pezzella, M.; Meuwly, M. O₂ formation in cold environments. *Phys. Chem. Chem. Phys.* **2019**, *21*, 6247–6255.
- (19) Pezzella, M.; Koner, D.; Meuwly, M. Formation and Stabilization of Ground and Excited-State Singlet O₂ upon Recombination of ³P Oxygen on Amorphous Solid Water. *J. Phys. Chem. Lett.* **2020**, *11*, 2171–2176.
- (20) Stief, L. J.; Payne, W. A.; Klemm, R. B. A flash photolysis–resonance fluorescence study of the formation of O(¹D) in the photolysis of water and the reaction of O(¹D) with H₂, Ar, and He-. *J. Chem. Phys.* **1975**, *62*, 4000–4008.
- (21) Garstang, R. Energy levels and transition probabilities in p 2 and p 4 configurations. *Mon. Not. R. Astron. Soc.* **1951**, *111*, 115–124.

- (22) Schmidt, F.; Swiderek, P.; Bredehoft, J. H. Formation of Formic Acid, Formaldehyde, and Carbon Dioxide by Electron-Induced Chemistry in Ices of Water and Carbon Monoxide. *ACS Earth Space Chem.* **2019**, *3*, 1974–1986.
- (23) Shimanouchi, T.; Matsuura, H.; Ogawa, Y.; Harada, I. Tables of molecular vibrational frequencies. *J. Phys. Chem. Ref. Data* **1978**, *7*, 1323–1444.
- (24) Unke, O. T.; Meuwly, M. Toolkit for the Construction of Reproducing Kernel-Based Representations of Data: Application to Multidimensional Potential Energy Surfaces. *J. Chem. Inf. Model.* **2017**, *57*, 1923–1931.
- (25) Dubrin, J.; MacKay, C.; Pandow, M.; Wolfgang, R. Reactions of atomic carbon with π -bonded inorganic molecules. *J. Inorg. Nuc. Chem.* **1964**, *26*, 2113–2122.
- (26) Xantheas, S. S.; Ruedenberg, K. Potential energy surfaces of carbon dioxide. *Int. J. Quant. Chem.* **1994**, *49*, 409–427.
- (27) Rosenblatt, M. Remarks on Some Nonparametric Estimates of a Density Function. *Ann. Math. Statist.* **1956**, *27*, 832–837.
- (28) Hama, T.; Yokoyama, M.; Yabushita, A.; Kawasaki, M. Role of OH radicals in the formation of oxygen molecules following vacuum ultraviolet photodissociation of amorphous solid water. *J. Chem. Phys.* **2010**, *133*, 104504.
- (29) Koner, D.; Bemish, R. J.; Meuwly, M. The $C(^3P) + NO(X^2\Pi) \rightarrow O(^3P) + CN(X^2\Sigma^+)$, $N(^2D)/N(^4S) + CO(X^1\Sigma^+)$ reaction: Rates, branching ratios, and final states from 15 K to 20 000 K. *J. Chem. Phys.* **2018**, *149*, 094305.
- (30) Davidson, J. A.; Schiff, H. I.; Brown, T. J.; Howard, C. J. Temperature dependence of the deactivation of $O(^1D)$ by CO from 113 to 333 K. *J. Chem. Phys.* **1978**, *69*, 1216–1217.

- (31) Ogryzlo, E.; Reilly, J.; Thrush, B. Vibrational excitation of CO from the reaction C+O₂. *Chem. Phys. Lett.* **1973**, *23*, 37–39.
- (32) Braunstein, M.; Duff, J. W. Electronic structure and dynamics of O(³P)+CO(¹Σ⁺) collisions. *J. Chem. Phys.* **2000**, *112*, 2736–2745.
- (33) Yan, C.; Teng, C. C.; Chen, T.; Zhong, H.; Rousso, A.; Zhao, H.; Ma, G.; Wysocki, G.; Ju, Y. The kinetic study of excited singlet oxygen atom O (1D) reactions with acetylene. *Comb. Flame* **2020**, *212*, 135–141.
- (34) Unke, O. T.; Meuwly, M. A reactive, scalable, and transferable model for molecular energies from a neural network approach based on local information. *J. Chem. Phys.* **2018**, *148*, 241708.
- (35) Unke, O. T.; Meuwly, M. PhysNet: A neural network for predicting energies, forces, dipole moments, and partial charges. *J. Chem. Theo. Comp.* **2019**, *15*, 3678–3693.
- (36) Unke, O. T.; Chmiela, S.; Sauceda, H. E.; Gastegger, M.; Poltavsky, I.; Schütt, K. T.; Tkatchenko, A.; Müller, K.-R. Machine learning force fields. *J. Chem. Theo. Comp.* **2021**,



TOC Graphic

Supplementary Information: Genesis of Polyatomic Molecules in Dark Clouds: CO₂ Formation on Cold Amorphous Solid Water

Meenu Upadhyay and Marco Pezzella and Markus Meuwly*

*Department of Chemistry, University of Basel, Klingelbergstrasse 80 , CH-4056 Basel,
Switzerland.*

E-mail: m.meuwly@unibas.ch

Methods

The Energy Functions

Reactive molecular dynamics simulations require potential energy surfaces (PESs) that allow bond formation and bond breaking.¹ Two such PESs were considered in the present work. One was based on fitting Morse potentials $V(r) = D_e(1 - \exp[-\beta(r - r_0)^2])$ to the C–O interaction based on *ab initio* calculations using the MOLPRO² suite of programs at the MRCI/aug-cc-pVTZ^{3,4} level of theory. The fitting parameters are $r_0 = 1.164 \text{ \AA}$, $D_0 = 173.50 \text{ kcal/mol}$, and $\beta = 2.53 \text{ \AA}^{-1}$. For the angular potential (the OCO bend) the parameters were those from the CHARMM36 force field⁵ and this PES is referred to as MMH (for Morse-Morse-Harmonic). Such an approach is similar to that used previously for oxygen-oxygen recombination on amorphous solid water.^{6,7}

The second ground state PESs is based on high-level CCSD(T)-F12⁸ calculations with the aug-cc-pVTZ-F12⁹ basis set using MOLPRO.² For the geometries, a grid of r , R , and θ values including $R \in [0.9, 5.9]\text{\AA}$, $r \in [0.8, 2.1]\text{\AA}$, and $\theta \in [0, 180]^\circ$ was used. In total, 7800 reference energies were determined and represented as a reproducing kernel Hilbert space.¹⁰ The root mean squared difference between the reference energies and the RKHS representation is 0.06 kcal/mol with $R^2 = 1.00$, see Figure S1.

For water the TIP3P model¹¹ was used and for CO₂ the partial charges were $q_{\text{O}} = -0.3e$ and $q_{\text{C}} = 0.6e$ with standard van der Waals parameters from CHARMM. These charges are consistent with those obtained from B3LYP/6-31G(d,p) calculations snapshots from the MD simulations with CO₂ adsorbed to the 10 nearest H₂O molecules which yield $q_{\text{C}} = 0.73e$ and $q_{\text{O}} = -0.35e$. Simulations starting from the reactant state (CO+O) were initialized with the same partial charges. This compares with charges of $q_{\text{C}} = 0.22e$ and $q_{\text{O}} = -0.21e$ for the CO molecule and $q_{\text{O}} = -0.1e$ for an oxygen atom adsorbed to the 10 nearest H₂O molecules. To assess the dependence of the results on the partial charges used, additional reactive MD simulations were carried out with $q_{\text{O}} = -0.1e$ and $q_{\text{C}} = 0.2e$ (i.e. $q_{\text{CO}} = 0.1e$) and with $q_{\text{O}} = -0.2e$ and $q_{\text{C}} = 0.4e$ (i.e. $q_{\text{CO}} = 0.2e$). In all cases, recombination was found to speed up considerably compared with $q_{\text{CO}} = 0.3e$ and $q_{\text{O}} = -0.3e$ due to the higher mobility of the CO molecule and the O atom on the ASW when reduced partial charges are used.

Although there are considerably more sophisticated models for water,^{12,13} simulations with the TIP3P model and point charges for atomic and molecular oxygen have yielded satisfactory agreement for diffusion coefficients for atomic oxygen on ASW with experiments.^{6,7,14,15} Similarly, adsorption of CO to the ASW as reported¹⁶ from simulations with a quadrupolar model for CO together with TIP4P is captured with the present parametrization. For temperatures up to $T = 100$ K, a) CO with charges $q_{\text{C}} = 0.22e$ and $q_{\text{O}} = -0.21e$ and b) $q_{\text{CO}} = 0.3e$ and $q_{\text{O}} = -0.3e$ remain physisorbed to the ASW surface on the nanosecond time

scale. Also, the more elaborate parametrizations, in particular for water, are computationally considerably more expensive and do not allow routine, multiple > 10 ns simulations to be carried out. As the main focus of the present work is on the CO+O recombination reaction the nonbonded models used here were deemed sufficient.

Molecular Dynamics Simulations

In the following, the coordinates are the CO stretch r , the separation R between the center of mass of CO_A and O_B and θ is the O_ACO_B angle. Hence $\theta = 0$ corresponds to the COO structure whereas $\theta = 180^\circ$ is the OCO conformation. Initial conditions were generated for a grid of angles $\theta \in [67.5, 78.75, 84.375, 90.0, 101.25, 112.5, 123.75, 135.0, 157.5, 180.0]^\circ$ and separations $R \in [2.66, 3.16, 3.66, 3.91, 4.16, 4.66, 5.16, 5.66]$ Å. A total of 80 initial simulations were carried out to obtain initial coordinates and velocities for each of the grid points. With constrained CO and O position first 750 steps of steepest descent and 100 steps Adopted Basis Newton-Raphson minimization was carried out, followed by 50 ps heating dynamics to 50 K. Then, 100 ps equilibration dynamics was carried out for 100 ps. From each of the runs coordinates and velocities were saved regularly to obtain 1000 initial conditions for each combination of angle and distance, i.e. in total 80000 initial conditions. Production simulations 250 ps in length were then run from saved coordinates and velocities with a time step of $\Delta t = 0.2$ fs in the NVE ensemble. Energy conservation demonstrating the correct implementation of the energies and forces for the reactive PESs is reported in Figure S2 for both, simulations with MMH and RKHS.

Table S1: List of observations from the simulations with the MMH potential for combination of angles and distances where R is the distance between CoM(CO) and O and θ is the angle between them.

$\theta(^{\circ})$	$R(\text{\AA})$	Total	CO ₂ formation	Atom exchange	No collision complex	ES1	ES2	Both desorb
67.5	2.66	100	0	0	1	2	3	94
78.75	2.66	500	6	20,17,12,6	107	96	23	213
78.75	3.16	500	0	22,18,6,17	9	8	14	406
78.75	3.66	100	0	1,3,3,2	2	8	0	81
84.375	2.66	500	36	89,25,21,45	47	37	44	156
84.375	3.16	100	1	2,6,2,2	7	2	6	72
84.375	3.66	100	0	6,7,4,5	6	6	1	65
90.0	2.66	1000	179	73,40,32,64	44	60	48	460
90.0	3.16	100	2	10,8,2,4	8	3	1	62
90.0	3.66	100	0	4,6,2,4	8	7	0	69
90.0	3.91	100	0	7,6,4,2	22	6	2	51
90.0	5.66	500	0	0	0	500	0	0
101.25	2.66	1000	751	44,37,9,4	0	21	5	129
101.25	3.16	100	8	11,5,2,9	20	6	3	36
101.25	3.66	500	14	41,27,24,16	66	52	19	241
101.25	3.91	300	7	23,13,10,3	97	33	8	106
101.25	4.16	100	0	1,0,1,1	88	3	2	4
101.25	4.66	100	0	0	99	0	0	1
112.5	2.66	1000	913	19,2,1,0	46	9	4	6
112.5	3.16	500	205	76,20,10,12	73	30	12	62
112.5	3.66	200	42	34,11,4,8	18	15	6	62
112.5	3.91	200	33	24,10,6,4	44	16	8	55
112.5	4.16	500	11	5,4,3,1	441	1	11	23
123.75	2.66	1000	998	0,1,0,0	0	0	0	1
123.75	3.16	100	79	9,0,0,0	7	2	1	2
123.75	3.66	100	44	16,3,3,3	7	5	3	16
123.75	3.91	100	32	17,3,2,1	14	3	11	17
123.75	4.16	100	8	4,1,0,1	84	0	0	2
123.75	4.66	100	0	0	100	0	0	0
135.0	2.66	1000	1000	0	0	0	0	0
135.0	3.16	1000	789	169,4,5,8	15	6	2	2
135.0	3.66	500	349	97,3,5,5	20	11	3	7
135.0	3.91	500	339	73,1,1,1	22	4	46	13
135.0	4.16	1000	167	14,1,2,6	253	35	378	144
135.0	4.66	1000	69	0	901	0	27	3
135.0	5.16	1000	0	0	1000	0	0	0
135.0	5.66	1000	0	0	1000	0	0	0

Table S2: Continuation of Table S1.

$\theta(^{\circ})$	$R(\text{\AA})$	Total	CO ₂ formation	Atom exchange	No collision complex	ES1	ES2	Both desorb
157.5	2.66	1000	1000	0	0	0	0	0
157.5	3.16	500	500	0	0	0	0	0
157.5	3.66	1000	997	0	1	0	1	1
157.5	3.91	500	494	0	3	0	2	1
157.5	4.16	500	242	0	233	0	24	1
157.5	4.66	500	0	0	500	0	0	0
157.5	5.66	100	0	0	100	0	0	0
180.0	2.66	1000	1000	0	0	0	0	0
180.0	3.16	1000	1000	0	0	0	0	0
180.0	3.66	1000	1000	0	0	0	0	0
180.0	3.91	1000	991	0	9	0	0	0
180.0	4.16	500	491	0	5	3	0	1
180.0	4.66	100	0	0	100	0	0	0
180.0	5.66	1000	0	0	1000	0	0	0

In the atom exchange column, labels (a, b, c, and d) refer to trajectories with atom exchange followed by a: CO and O remain on the surface, b: CO and O desorb, c: O remains on surface and CO desorbs, and d: CO remains on surface and O desorbs.

Table S3: List of observations from the simulations using the 3d RKHS PES where R is the distance between CoM(CO) and O and θ is the angle between them.

$\theta(^{\circ})$	$R(\text{\AA})$	Total	CO ₂ formation	Atom exchange	No collision complex	ES1	ES2	Both desorb	COO formation
67.5	2.66	100	17	0	0	0	1	82	0
78.75	2.66	100	51	0	3	1	0	45	0
78.75	3.16	100	4	0	0	0	0	2	94
78.75	3.66	100	0	0	89	1	0	0	10
84.375	2.66	100	62	0	2	5	3	27	1
84.375	3.16	100	6	0	0	0	0	0	94
84.375	3.66	100	0	0	96	2	0	0	2
90.0	2.66	100	97	0	3	0	0	0	0
90.0	3.16	100	45	0	5	0	0	0	50
90.0	3.66	100	0	0	0	97	0	0	3
101.25	2.66	100	100	0	0	0	0	0	0
101.25	3.16	100	97	0	3	0	0	0	0
101.25	3.66	100	0	0	96	3	0	0	1
112.5	2.66	100	100	0	0	0	0	0	0
112.5	3.16	100	100	0	0	0	0	0	0
112.5	3.66	100	4	0	93	0	1	2	0
112.5	3.91	100	0	0	94	4	1	0	1
123.75	2.66	100	100	0	0	0	0	0	0
123.75	3.16	100	100	0	0	0	0	0	0
123.75	3.66	100	5	0	93	0	0	2	0
123.75	3.91	100	0	0	93	4	1	0	2
135.0	2.66	100	100	0	0	0	0	0	0
135.0	3.16	100	100	0	0	0	0	0	0
135.0	3.66	500	46	0	393	0	56	0	5
135.0	3.91	1000	1	0	731	9	242	0	17
135.0	4.16	100	0	0	97	0	0	0	3
157.5	2.66	100	100	0	0	0	0	0	0
157.5	3.16	100	100	0	0	0	0	0	0
157.5	3.66	100	12	0	59	0	28	0	1
157.5	3.91	100	0	0	76	0	19	0	5
180.0	2.66	1000	1000	0	0	0	0	0	0
180.0	3.16	100	99	0	0	0	0	1	0
180.0	3.66	500	53	0	292	2	135	8	10
180.0	3.91	100	1	0	99	0	0	0	0
180.0	4.16	100	0	0	93	0	5	1	1

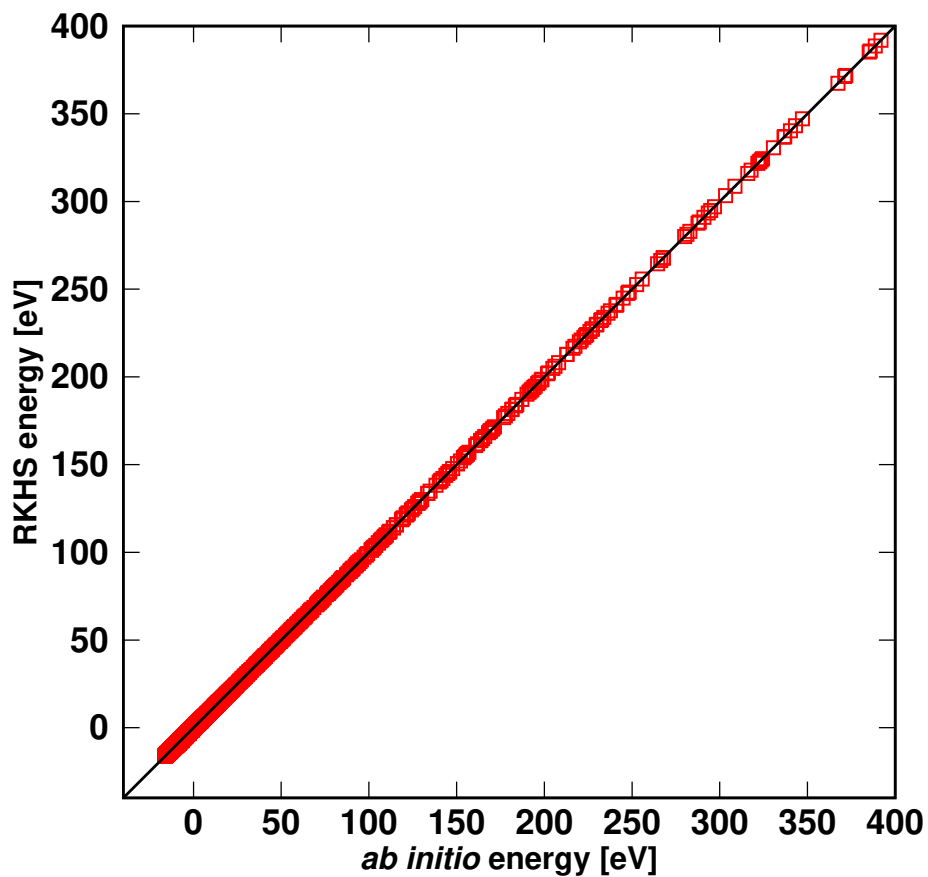


Figure S1: Quality of the RKHS representation for the CCSD(T)-F12 points from the electron structure calculations. The RMSE is 0.0026 eV (0.06 kcal/mol) and the $R^2 = 1.0$.

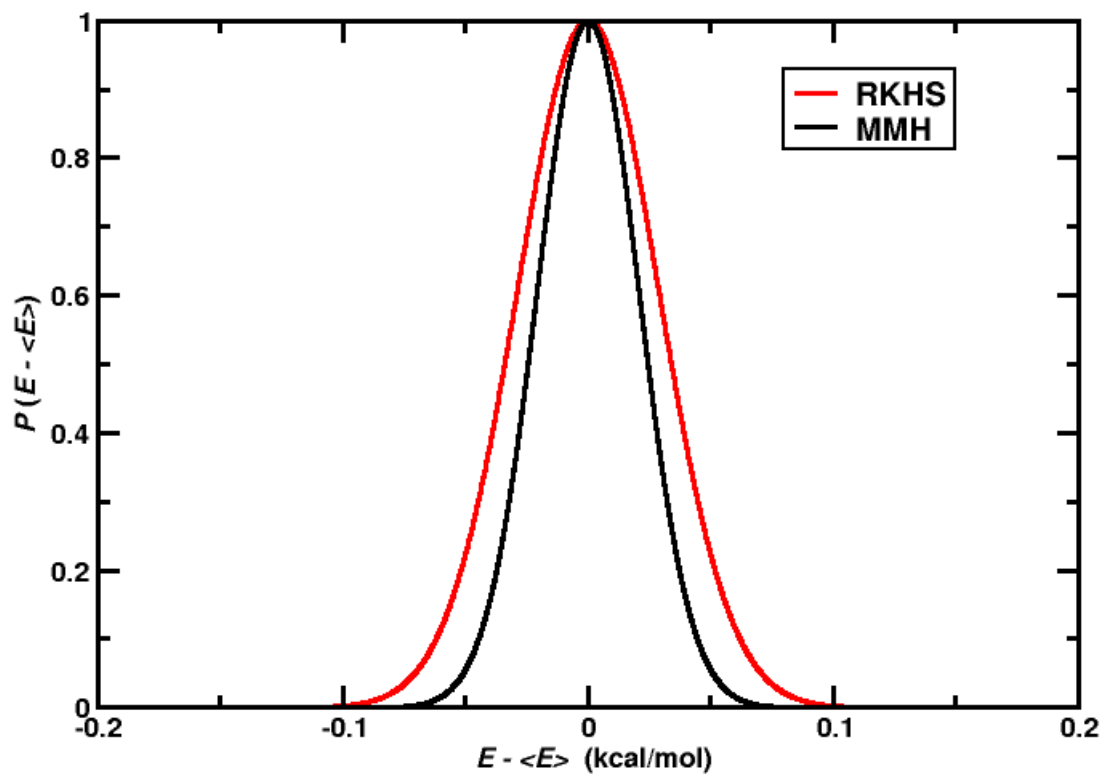


Figure S2: Energy conservation for a reactive simulation using MMH (black) and the RKHS representation of the CCSD(T)-F12 calculations (red). The Gaussian shape of the curve confirms the energy conservation.

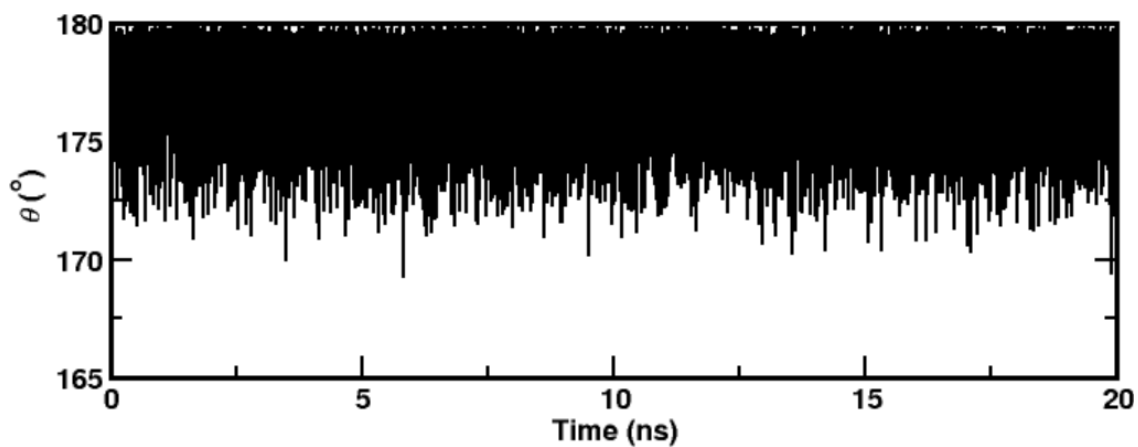


Figure S3: Time series for $\theta(t)$ from 20 ns simulation, reporting the raw data of Figure 3B

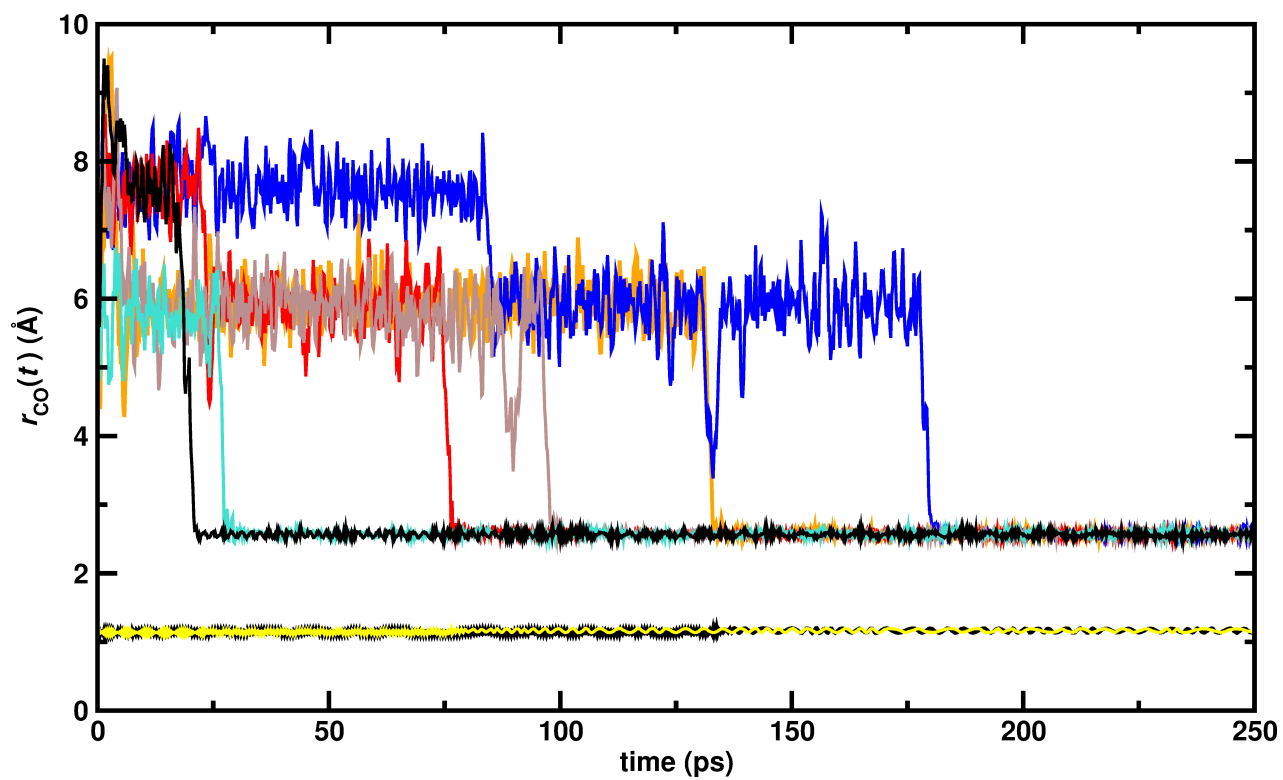


Figure S4: Time series for rebinding into the COO conformation from simulations using the RKHS PES.

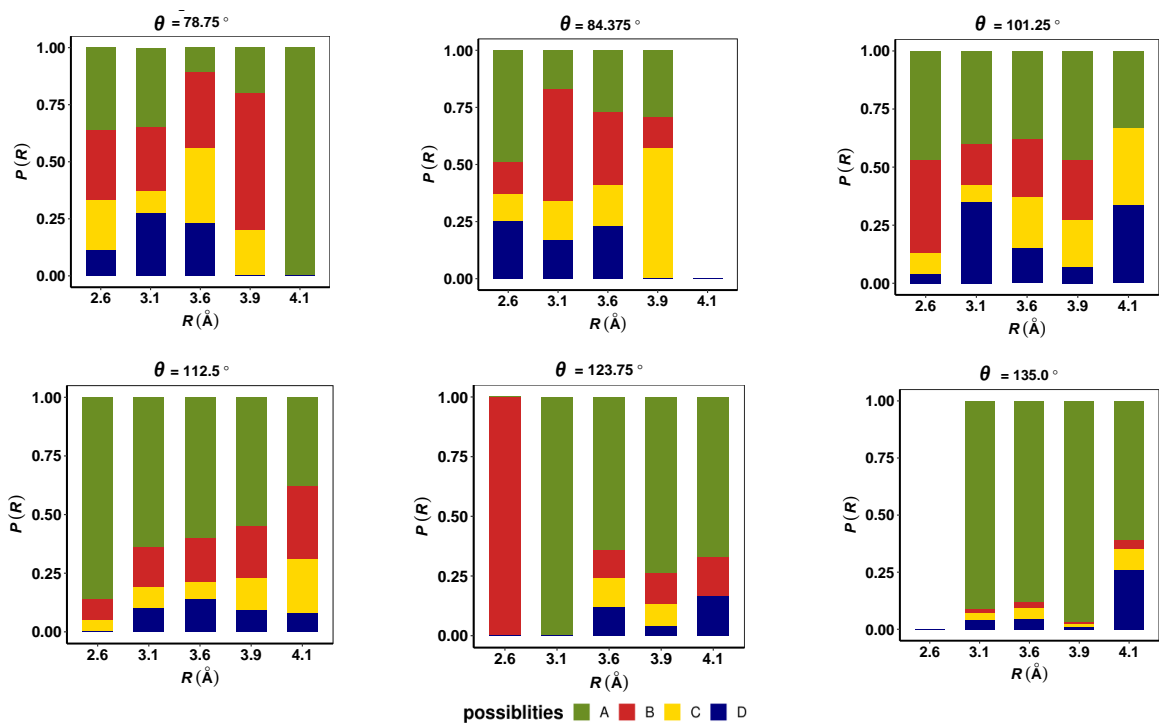


Figure S5: After atom exchange, there are 4 further possibilities i.e both CO and O remains on the water surface (A), both CO and O desorbs (B), O remains and CO desorbs (C), CO remains and O desorbs (D) from water surface. Plots for atom exchange probability for each of the grid points using MMH.

References

- (1) T. Nagy, J. Y. R.; Meuwly, M. Multi-Surface Adiabatic Reactive Molecular Dynamics. *J. Chem. Theo. Comp.* **2014**, *10*, 1366–1375.
- (2) Werner, H.-J. et al. The Molpro quantum chemistry package. *J. Chem. Phys.* **2020**, *152*.
- (3) Werner, H.-J.; Knowles, P. J. An efficient internally contracted multiconfiguration–reference configuration interaction method. *J. Chem. Phys.* **1988**, *89*, 5803–5814.
- (4) Dunning Jr, T. H. Gaussian basis sets for use in correlated molecular calculations. I. The atoms boron through neon and hydrogen. *J. Chem. Phys.* **1989**, *90*, 1007–1023.
- (5) Best, R. B.; Zhu, X.; Shim, J.; Lopes, P. E.; Mittal, J.; Feig, M.; MacKerell Jr, A. D. Optimization of the additive CHARMM all-atom protein force field targeting improved sampling of the backbone ϕ , ψ and side-chain χ_1 and χ_2 dihedral angles. *J. Chem. Theo. Comp.* **2012**, *8*, 3257–3273.
- (6) Pezzella, M.; Meuwly, M. O₂ formation in cold environments. *Phys. Chem. Chem. Phys.* **2019**, *21*, 6247–6255.
- (7) Pezzella, M.; Koner, D.; Meuwly, M. Formation and Stabilization of Ground and Excited-State Singlet O₂ upon Recombination of ³P Oxygen on Amorphous Solid Water. *J. Phys. Chem. Lett.* **2020**, *11*, 2171–2176.
- (8) Adler, T. B.; Knizia, G.; Werner, H.-J. A simple and efficient CCSD(T)-F12 approximation. 2007.
- (9) Peterson, K. A.; Adler, T. B.; Werner, H.-J. Systematically convergent basis sets for explicitly correlated wavefunctions: The atoms H, He, B–Ne, and Al–Ar. *J. Chem. Phys.* **2008**, *128*, 084102.

- (10) Unke, O. T.; Meuwly, M. Toolkit for the Construction of Reproducing Kernel-Based Representations of Data: Application to Multidimensional Potential Energy Surfaces. *J. Chem. Inf. Model.* **2017**, *57*, 1923–1931.
- (11) Jorgensen, W. L.; Chandrasekhar, J.; Madura, J. D.; Impey, R. W.; Klein, M. L. Comparison of simple potential functions for simulating liquid water. *J. Chem. Phys.* **1983**, *79*, 926–935.
- (12) Wang, L.-P.; Head-Gordon, T.; Ponder, J. W.; Ren, P.; Chodera, J. D.; Eastman, P. K.; Martinez, T. J.; Pande, V. S. Systematic improvement of a classical molecular model of water. *J. Phys. Chem. B* **2013**, *117*, 9956–9972.
- (13) Devereux, M.; Pezzella, M.; Raghunathan, S.; Meuwly, M. Polarizable Multipolar Molecular Dynamics Using Distributed Point Charges. *J. Chem. Theo. Comp.* **2020**, *16*, 7267–7280.
- (14) Lee, M. W.; Meuwly, M. Diffusion of atomic oxygen relevant to water formation in amorphous interstellar ices. *Faraday Discuss.* **2014**, *168*, 205–222.
- (15) Pezzella, M.; Unke, O. T.; Meuwly, M. Molecular Oxygen Formation in Interstellar Ices Does Not Require Tunneling. *J. Phys. Chem. Lett.* **2018**, *9*, 1822–1826.
- (16) Arasa, C.; van Hemert, M. C.; van Dishoeck, E. F.; Kroes, G.-J. Molecular Dynamics Simulations of CO₂ Formation in Interstellar Ices. *J. Phys. Chem. A* **2013**, *117*, 7064–7074.